Consistent Nonlinear Estimation of Longitudinal Tire Stiffness and Effective Radius

Christopher R. Carlson, Ph.D., Stanford University, crcarlson@stanfordalumni.org, and J. Christian Gerdes, Assistant Professor, Stanford University, gerdes@cdr.stanford.edu

***Abstract*— This paper presents two effectively unbiased nonlinear estimation schemes which identify tire longitudinal stiffness and effective radius using GPS and ABS wheelspeed sensors. A nonlinear approach is taken as one possible approach of eliminating the well known biases that linear least squares algorithms introduce for this problem. These new estimation strategies are then used to experimentally identify the longitudinal stiffness and effective radius of a summer tire and a winter tire under several different test conditions. The data clearly shows that there are several important parameters which govern tire longitudinal stiffness behavior in the low slip region. At a minimum, inflation pressure, tread depth, normal loading and temperature have a strong influence on longitudinal stiffness estimates; the change from dry to wet asphalt had the smallest effect on longitudinal stiffness estimates.**

***Index Terms*— GPS, total least squares, estimation, longitudinal stiffness, slip, road friction, tire, tire pressure, effective radius**

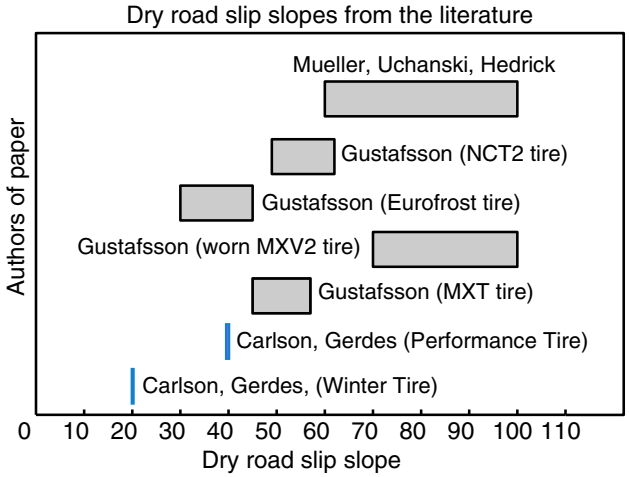

Fig. 1. Dry road slip slopes from the literature with more than one data set [8] and slip slopes from the current work for comparison

I. Introduction

SEVERAL research groups propose peak road friction estimation schemes under the premise that tire longitudinal stiffness for low values of slip indicates the peak value of the force slip curve [1], [2], [3], [4], [5], [6], [7], [8], [9]. Other groups seek to identify peak road friction coefficient with vehicle dynamics models and observers [10], [11]. Peak road friction information could be valuable for a number applications such as driver assistance [12] and stability control systems which use force based tire models [13].

Although a physical explanation is still lacking, during experiment longitudinal stiffness does appear to depend on the peak road friction coefficient. However, the current longitudinal slip estimation schemes demonstrated in the literature return a wide range of stiffness estimates for nominally similar conditions. Typical parameter variation ranges from 20% to 100% for individual tires on a relative scale and by up to an order of magnitude across all tires on an absolute scale [8].

Figure 1 shows variability of longitudinal stiffness estimates from the literature and their spread in terms of the slip slope. The slip slope is the longitudinal stiffness estimate normalized by the weight acting on the tire. The width of each band shows the range of estimates for different test conditions.

One factor which contributes to this variation for some formulations is the nonlinear nature of the force-slip equation. Although linear in the parameters, the equation is nonlinear in the measurements. The potential for parameter bias for this system structure is well known [14], and for this application section III shows it is insidious even in simulation.

It is also well known that tire longitudinal stiffness exhibits strong sensitivity to a wide variety of operating conditions such as temperature, inflation pressure, normal loading, tread depth [15] and possibly surface condition. Isolating one of these effects from a single lumped parameter is quite difficult. Some groups propose online adaptation methods which identify changes in stiffness [3]. Another group looked to tire lateral stiffness for a stronger measurement signal and less sensitivity to some operating conditions [16].

This work develops an extremely consistent parameter estimator for longitudinal slip and wheel effective radius. It then uses this estimator to study the relative effects of several driving conditions upon the tire parameters using stock vehicle ABS sensors and GPS. Section II discusses the vehicle and tire models used for this work. Section III discusses the pitfalls of using linear estimators for this problem structure. Section IV introduces a nonlinear estimator and its philosophical motivation. Section V discusses implementation details of the proposed algorithms and demonstrates their effectiveness using simulation studies. Section VI describes the experimental procedures, test matrix and presents the results.

II. Modeling

A. Tire model

The SAE definition for wheel slip is:

$$\text{Slip} \quad = \quad -\left(\frac{V - R\omega}{V}\right) \tag{1}$$

Where V is the velocity of the center of the tire, R is the effective radius of the tire and ω is angular velocity of the tire. The relationship between the force and slip for different tire models is the subject engineering modeling preference. Empirical tire models such as the Magic Formula [17] model the relationship between force transmitted by the tire and the resulting slip with complicated nonlinear relationships. Figure 2 shows typical force-slip curves of the Magic Formulae for different values of road surface to tire friction. The HSRI tire model [18] used

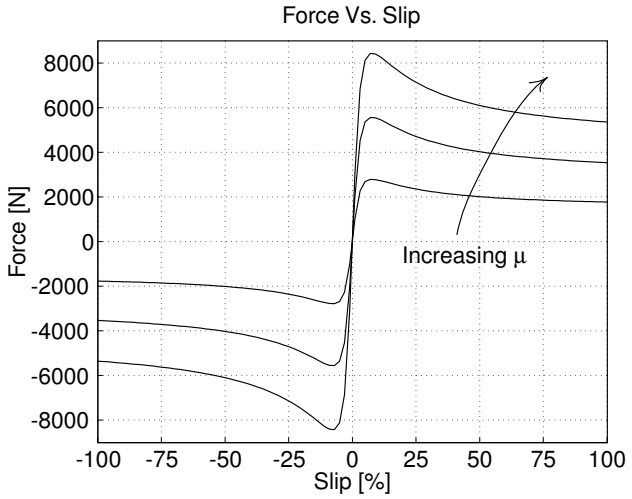

Fig. 2. Magic Formula tire model curves for increasing μ

in production stability control systems [19] shows curves with different qualitative shape.

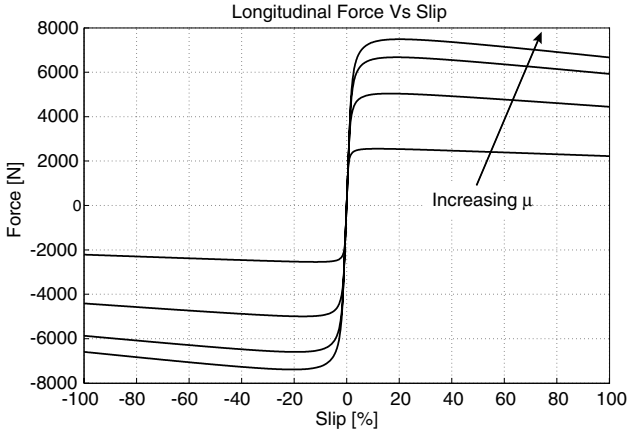

Fig. 3. HSRI tire model for different values of μ

During ordinary driving, the tire slip rarely exceeds 1-2%. By linearizing the either model in this small region, the force slip relation can be characterized as:

$$F = C_x \left(\frac{V - R\omega}{V} \right) \quad (2)$$

Where F and C_x are the force and longitudinal stiffness of the tire(s) transmitting the force.

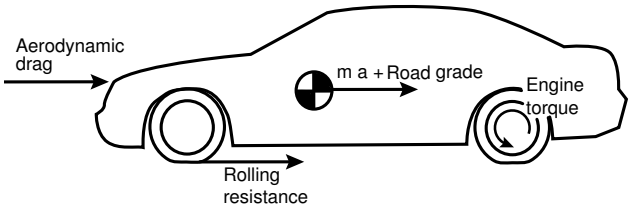

Fig. 4. Force diagram for test vehicle

B. Force Estimation

The dominant efforts acting on the tires during normal driving are illustrated in figure 4.

$$ma = F_x - F_{rr} - F_d - mg\sin(\theta) \quad (3)$$

Where F_x is the longitudinal force from the powertrain, F_{rr} is the rolling resistance, F_d is the aerodynamic drag and $mg\sin\theta$ is the contribution of road grade with angle θ. The rolling resistance, aerodynamic drag and road grade may be estimated using GPS and automotive sensors under normal driving conditions [20]. Since the referenced parameter estimation schemes do require sufficient excitation to converge, for instance at constant velocity the mass parameter is unobservable, the longitudinal stiffness estimation schemes makes use of the previous best estimate of the model parameters and updates the model when new information becomes available. During normal driving, accelerating to driving speeds from a stoplight, or accelerating to freeway speeds while merging should yield enough excitation for a new parameter update. Although this scheme may not provide instantaneous parameter updates when they are ideally needed, it is certainly better than assuming the values a priori.

The work appearing in this paper simplifies the force balance to eliminate as many testing uncertainties as is possible. Vehicle testing is performed on flat roads to eliminate the effect of road grade. Speed is kept below $15[m/s]$ to minimize the forces due to aerodynamic drag and the engine forces are kept high with respect to the neglected terms. During these testing conditions the forces transmitted by the tires are assumed to be inertial forces and they are estimated by multiplying the vehicle mass by the acceleration at the center of gravity. Therefore only the averaged driven tire parameters are identified. As stated it is not possible to identify the longitudinal stiffness and effective radius of the undriven wheels, and high speeds as well as a nonzero road grade would disrupt the measurement. Furthermore the vehicle must be accelerating or decelerating for the longitudinal stiffness parameter to be observable. The advantage of these experimental simplifications is to focus the attention upon tire parameter estimation and not upon the intricacies of vehicle external force estimation.

C. Vehicle Velocity Estimation

Until recently it has been difficult to measure absolute vehicle velocity accurately. Inertial measurement based observers were proposed in [10]. Work in [21] and [22] discuss the advantages of using Global Positioning System (GPS) velocity

as an absolute velocity sensor for measuring slip. While GPS velocity could be used directly, this paper assumes the vehicle is rear wheel drive and that the front wheels are free to roll at all times and thus the vehicle velocity is,

$$V = R_u \dot{\theta_u} \quad (4)$$

where R_u is the undriven wheel free-rolling radius and θ_u is undriven wheel angular displacements measured by an ABS variable reluctance sensor. R_u is assumed constant and is estimated separately using GPS. The time derivatives of the wheel angle measurements θ_x are not directly available and are estimated as

$$\hat{\dot{\theta}}_x = \frac{\hat{\theta}_x^{k+1} - \hat{\theta}_x^{k-1}}{2T} \quad (5)$$

Where $\hat{\theta}_x$ is the measured front or rear wheel angle measurement and T is the sampling time. For the remainder of this paper, the subscript u will refer to the undriven wheel and the subscript d will refer to the driven wheel.

This mildly indirect velocity measurement has the practical disadvantage that the estimation scheme can not be applied to the standard case of four wheel braking. However, it has the physical advantage of using only the ABS sensors for acceleration, velocity and position information. This simplifies the estimation algorithm proposed in Section IV by constraining the error sources to have the same error distributions.

The undriven wheel radius is the estimeate with a simple least squares regression of the form,

$$R_u = \begin{bmatrix} \hat{\dot{\theta}}(0) \\ \hat{\dot{\theta}}(T) \\ \vdots \\ \hat{\dot{\theta}}((N-1)T) \end{bmatrix}^{\dagger} \begin{bmatrix} V_{GPS}(0) \\ V_{GPS}(T) \\ \vdots \\ V_{GPS}((N-1)T) \end{bmatrix} \quad (6)$$

where the † notation refers to the psudoinverse of a matrix, T represents the sample period and N reflects the number of samples. When operating on about 60 seconds of constant velocity data at a 10[Hz] sample rate, this scheme yields consistently repeatable estimates of R_u which physically lies between the measured static unloaded wheel radius and the measured loaded wheel radius.

III. Linear Estimation Algorithms

A. Force Formulation

Previous work in [22] estimates the driven tire parameters C_x and R_d by formulating equation 2 as a linear regression:

$$\hat{a} = \begin{bmatrix} -\frac{1}{m} & \frac{\hat{\omega}_d}{m\hat{V}} \end{bmatrix} \begin{bmatrix} C_x \\ R_d C_x \end{bmatrix} \quad (7)$$

Where m is the mass of the vehicle, R_d is the effective radius of the driven wheel and $\hat{a}, \hat{\omega}_d, \hat{V}$ represent vehicle acceleration, front wheel angular velocity and vehicle velocity. The $\hat{}$ notation represents measured values or values calculated from measurements.

One way to interpret this formulation is that the estimator is seeking to minimize the force error in the least squares sense, which is not the same as minimizing the measurement errors. With measurement perturbations the equation becomes:

$$a + \Delta a = \begin{bmatrix} -\frac{1}{m} & \frac{\omega_d + \Delta\omega_d}{m(V+\Delta V)} \end{bmatrix} \begin{bmatrix} C_x \\ R_d C_x \end{bmatrix} \quad (8)$$

Where the Δ parameters represent measurement perturbations. Rearranging the deterministic and stochastic parts:

$$a - \begin{bmatrix} -\frac{1}{m} & \frac{\omega_d}{mV} \end{bmatrix} \begin{bmatrix} C_x \\ R_d C_x \end{bmatrix} = -\Delta a + \begin{bmatrix} 0 & \Delta\left(\frac{\omega_d}{mV}\right) \end{bmatrix} \begin{bmatrix} C_x \\ R_d C_x \end{bmatrix} \quad (9)$$

where,

$$\Delta\left(\frac{\omega_d}{mV}\right) = \frac{V\Delta\omega_d - \omega_d \Delta V}{m(V+\Delta V)V} \quad (10)$$

Although linear in the parameters, equation 7 does not observe *all* of the assumptions of least squares estimation and will lead to biased parameter estimates. In particular, it incorporates measurements in the second column of the estimation matrix. This is well known to introduce parameter biases except for very special noise structures [14]. Explicitly separating the noise terms from the measurements as in equation 9 intuitively shows how the multiplicative $\Delta\left(\frac{\omega_d}{mV}\right)$ errors will tend to bias the parameter estimates. The larger the $R_d C_x$ parameter, the larger the noise contribution from the measurement error in the second column becomes. Since least squares seeks to minimize the equation error, this will tend to encourage the estimator to make the parameter $R_d C_x$ artificially small. Although violating this assumption does not always lead to severely biased estimates, for this particular problem estimation problem, Section V-C demonstrates that the parameter biases can be very large for small measurement noise values.

B. Linear Energy Form

In an effort to limit the noise introduced by finite differencing the wheel angular position measurements necessary for the force formulation, equation 7 may be rewritten with an energy interpretation.

$$\begin{aligned} m\frac{dV}{dt} &= -C_x\left(\frac{V - R\omega}{V}\right) \\ m\int V dV &= -C_x \int (V - R\omega) dt \\ mV^2 - mV_0^2 &= -2C_x(S - R\theta) \end{aligned}$$

This equation equates the kinetic energy added to the vehicle to the longitudinal stiffness multiplied by the slipped distance of the drive tire.

Substituting equation 4 into the energy equation above and letting θ_d, R_d be the driven wheel angle and radius respectively yields:

$$mR_u^2\left(\dot{\theta_u}^2 - \dot{\theta_{u0}}^2\right) = -2C_x(R_u\theta_u - R_d\theta_d) \quad (11)$$

Which assumes that the driven wheel provides all the force on the vehicle and the undriven wheel always stays free to roll. In particular, this means that the vehicle does not brake during the maneuver.

Once again approximating the time derivatives as finite difference equations and forming a linear regression similar to equation 7.

$$mR_u^2\left(\dot{\hat{\theta}}_u^{\ 2} - \dot{\hat{\theta}}_{u0}^{\ 2}\right) = -2\left[\ R_u\hat{\theta}_u\ \ -\hat{\theta}_d\ \right]\left[\begin{array}{c} C_x \\ R_dC_x \end{array}\right]$$

Although the double difference has been eliminated and the single differencing has been reduced, the parameters are still biased using this linear estimation structure. The following section shows that even for small noise magnitudes, the bias can still be quite large for this formulation.

C. Linear Truth Simulation

The large biases inherent to the linear formulations are demonstrated by a continuous time simulation which models force, velocity and slip using equation 1. All other dynamics such as vehicle pitch and tire deformation are ignored. The errors of the wheel angular displacement signals are modeled as white noise which is added to the simulated sensor measurements. The standard deviations used to model the noise of the wheelspeed measurements is $0.04[rad]$ which is less than the resolution of the wheel angle sensor $[100counts/rev]$. The simulated vehicle accelerates at $3[m/s^2]$ and decelerates at $-1[m/s^2]$ for times which yield an average velocity of $13[m/s]$. These accelerations are physically realizable by our test vehicle and were chosen to mimic accelerations and velocities during data collection conditions which appear later in this paper. Figure 5 shows a representative set of simulation data.

Figure 6 illustrates parameter estimation results of twenty simulated data sets. The force formulation consistently underestimates the longitudinal stiffness by about a factor of 5, while the energy form tends to over estimate the stiffness by about 50%. It is interesting to note that the wheel radius is consistently estimated to submillimeter accuracy by both linear estimation schemes despite the large variation in longitudinal stiffness.

If these linear schemes fail to provide reasonable parameter estimates for such idealized simulation studies, it is highly unlikely they will perform better for real data. This suggests a new approach is needed to solve this problem.

IV. Nonlinear Formulations

In the spirit of a least squares solution, the optimization problems presented here seek to minimize the *measurement errors* $[\Delta\theta_d^T\Delta\theta_u^T]^T$ in the driven and undriven wheel angle measurements θ_d and θ_u. The philosophy of this optimization is called, *orthogonal regression*, *errors in the variables* (EIV) or more recently a *Total Least Squares* (TLS) problem. For linear systems, this data analysis technique yields strongly consistent, asymptotically unbiased parameter estimates if the noise on the variables are independent and identically distributed (IID) with equal or known variances [23]. The problems above are posed using two identical sensors. Although these sensors are coupled through the dynamics of the vehicle, their error variances are virtually identical and in practice and simulation their errors do not appear to be correlated.

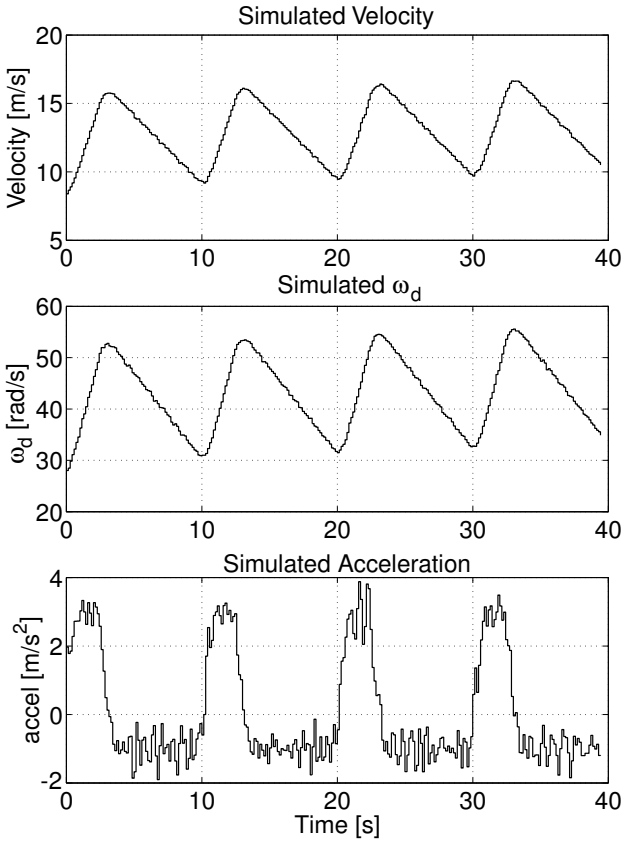

Fig. 5. Typical truth simulation velocity, ω_d and acceleration

Both the energy and force formulations may be manipulated into this form.

A. Nonlinear Force Form

Explicitly introducing measurement noise perturbations into equation 2 yields:

$$mR_u(\theta_u + \ddot{\Delta\theta}_u) = -C_x\left(\frac{R_u(\theta_u + \dot{\Delta\theta}_u) - R_d(\theta_d + \dot{\Delta\theta}_d)}{R_u(\theta_u + \dot{\Delta\theta}_u)}\right)$$

Moving everything to the left hand side,

$$mR_u^2(\theta_u + \ddot{\Delta\theta}_u)(\theta_u + \dot{\Delta\theta}_u) + C_x\left(R_u(\theta_u + \dot{\Delta\theta}_u) - R_d(\theta_d + \dot{\Delta\theta}_d)\right) = 0 \qquad (12)$$

The solution to these problems will be iterative and the time derivatives are approximated by first order finite difference equations. Let each measurement be written as:

$$\hat{\theta}^k = \theta^k + \Delta\theta^k$$

then,

$$\dot{\hat{\theta}}^k \cong \frac{\hat{\theta}^{k+1} - \hat{\theta}^{k-1}}{2T} \qquad (13)$$

$$\ddot{\hat{\theta}}^k \cong \frac{\hat{\theta}^{k+2} - 2\hat{\theta}^k + \hat{\theta}^{k-2}}{4T^2} \qquad (14)$$

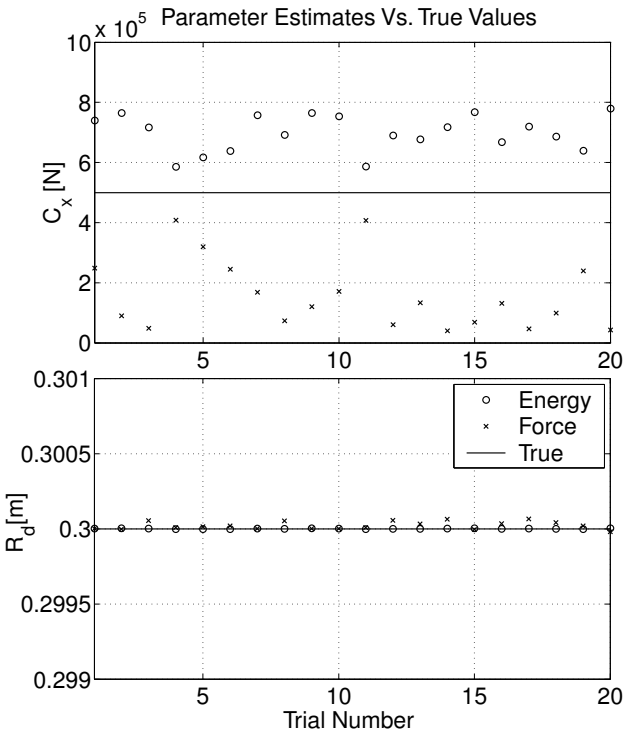

Fig. 6. Truth simulation for linear parameter estimation schemes

where k represents the discrete time step and T represents the digital sampling rate. Equation 12 can be written more conveniently as:

$$f^k(\hat{\theta}_u, \hat{\theta}_d, \Delta\theta_u, \Delta\theta_d, R_d, C_x) \quad = \quad 0$$

The goal of minimizing the sum of the squared measurement errors, which should yield the correct parameter estimates in the presence of Independent Identically Distributed (IID) noise, can then be stated:

$$\begin{aligned} &\text{Minimize: } \|[\Delta\theta_u^T \ \Delta\theta_d^T]^T\| \\ &\quad \text{Subject to: } f^k(\hat{\theta}_u, \hat{\theta}_d, \Delta\theta_u, \Delta\theta_d, R_d, C_x) = 0 \end{aligned} \qquad (15)$$

B. Nonlinear Energy Form

As above, introduce measurement noise perturbations into equation 11:

$$\begin{aligned} &mR_u^2(\theta_u + \dot{\Delta\theta_u})^2 - mR_u^2(\theta_{u0} + \dot{\Delta\theta_{u0}})^2 = \\ &\quad -2C_x(R_u(\theta_u + \Delta\theta_u) - R_d(\theta_d + \Delta\theta_d)) \end{aligned}$$

Which can be written as

$$\begin{aligned} &mR_u^2(\theta_u + \dot{\Delta\theta_u})^2 - mR_u^2(\theta_{u0} + \dot{\Delta\theta_{u0}})^2 + \\ &\quad 2C_x(R_u(\theta_u + \Delta\theta_u) - R_d(\theta_d + \Delta\theta_d)) \quad = \quad 0 \end{aligned}$$

Using the same time derivative approximation for the $\dot{\hat{\theta}}$ terms in equation 13, the above equation can be written:

$$g^k(\hat{\theta}_u, \hat{\theta}_d, \Delta\theta_u, \Delta\theta_d, R_d, C_x) \quad = \quad 0$$

Then, the goal of minimizing the sum of the squared measurement errors is stated:

$$\begin{aligned} &\text{Minimize: } \|[\Delta\theta_u^T \ \Delta\theta_d^T]^T\| \\ &\quad \text{Subject to: } g^k(\hat{\theta}_u, \hat{\theta}_d, \Delta\theta_u, \Delta\theta_d, R_d, C_x) = 0 \end{aligned} \qquad (16)$$

C. Cost Functions

Like many nonlinear estimation algorithms, such as extended kalman filters for example, a poor initial guess for the parameters could lead to poor convergence of the estimator. Fortunately the cost functions for these optimization problems are locally quasiconvex for physically meaningful parameter values as demonstrated in figures 7 and 8. As such once the true values are bracketed, a bisection is guaranteed to converge to the optimal solution. This algorithm was used with success previously in [24]. The following section shows how to cast these problems as nonlinear least squares problems which converge with significantly less computational effort.

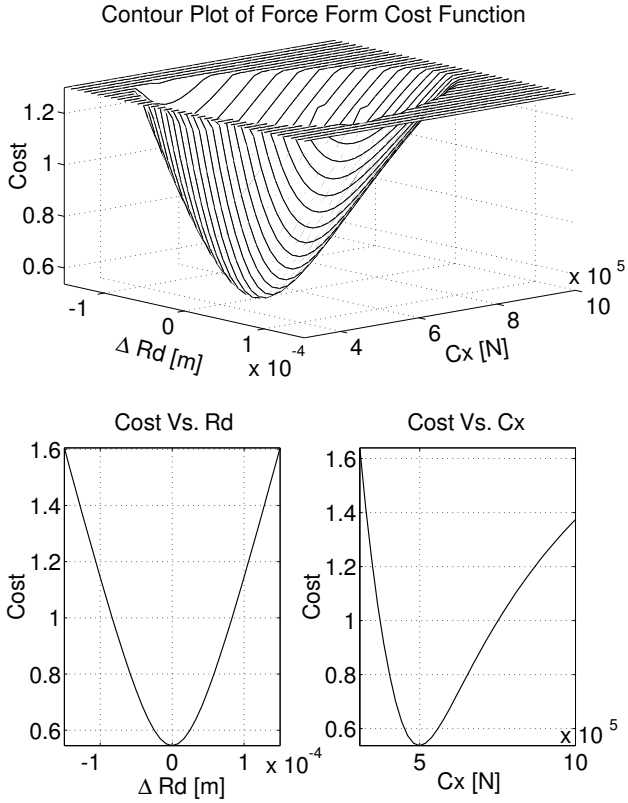

Fig. 7. Typical cost function for force formulation and cross sections

V. Nonlinear Estimation Algorithm

This section presents two improvements to the standard bisection algorithm. The first improvement is to reinterpret the problem as a nonlinear least squares problem which converges faster than the previously proposed algorithms, the second uses the sparce structure of the cost function gradient to speed up the required linear algebraic operations.

A. Nonlinear Total Least Squares

Bisection algorithms are guaranteed to converge for quasiconvex functions but may take many iterations to do so. A faster methodology for these problems solves the optimization problems as nonlinear total least squares (NLTLS) problems [23] with backstepping.

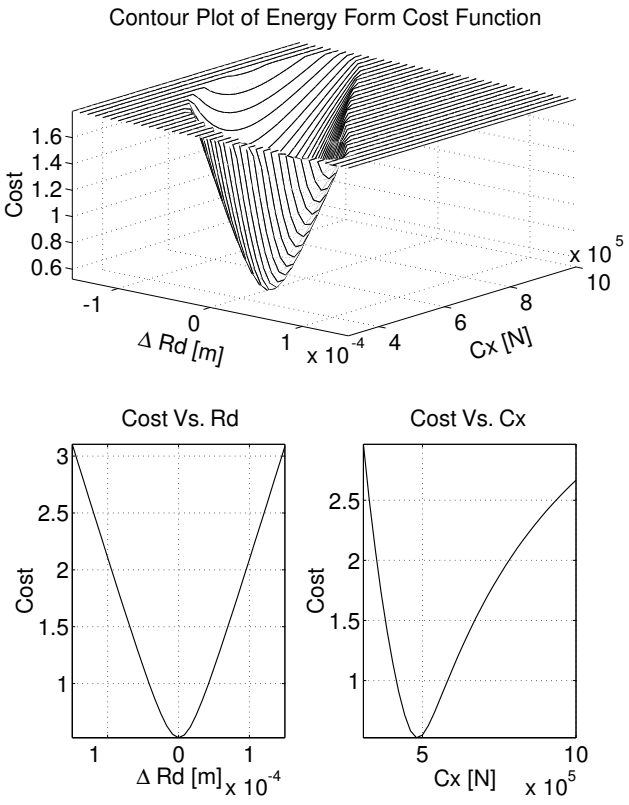

Fig. 8. Typical cost function for energy formulation and cross sections

Let f be the true nonlinear model:

$$f(a, x) = b \tag{17}$$

where a and b are vectors of true model values and x is a vector of parameters.

Assume that the vectors of measurements are disturbed by noise

$$\hat{a} = a + \Delta a \tag{18}$$
$$\hat{b} = b + \Delta b \tag{19}$$

Just as with ordinary least squares, if the sum of the squared measurement errors are minimized, the true parameter values will be returned. This may be written as a NLTLS problem,

$$\begin{array}{ll} \text{Minimize:} & \left\| \begin{array}{c} \Delta a \\ \Delta b \end{array} \right\| \\ x,\ \Delta a,\ \Delta b & \end{array} \tag{20}$$

$$\text{Subject to:} \quad f(\hat{a} - \Delta a, x) = \hat{b} - \Delta b \tag{21}$$

Problems of this form may be solved by writing an equivalent nonlinear least squares problem of higher dimension [25],

$$\begin{array}{ll} \text{Minimize:} & \left\| \begin{array}{c} f(a, x) - \hat{b} \\ a - \hat{a} \end{array} \right\| \\ a,\ x & \end{array} \tag{22}$$

Solutions to these problems iteratively approximate the nonlinear function as quadratic and solve a local linear least squares problem. To see this, let

$$\Theta = \left[\begin{array}{c} x \\ a \end{array} \right] \tag{23}$$

$$g(\Theta) = \left[\begin{array}{c} f(a, x) - \hat{b} \\ a - \hat{a} \end{array} \right] \tag{24}$$

Then iteratively solve the problem,

$$J^i = \left. \frac{\partial g(\Theta)}{\partial \Theta} \right|_{\Theta^i} \tag{25}$$

$$\Theta^{i+1} = \Theta^i + \alpha J^\dagger g^i(\Theta^i) \tag{26}$$

until the Θ^i converges, and where i refers to the iteration number, $\dagger$ represents the least squares pseudoinverse and $0 < \alpha < 1$ is the backstepping parameter. The initial conditions may be educated guesses, for this paper the routine starts with the linear least squares parameter estimates and zeros for the measurement errors. Typically the solution converges in less than ten iterations and a backstepping parameter of $\alpha = 0.8$ works well.

B. Exploiting Structure

The QR factorization (QRF) is a powerful tool for finding the pseudoinverses of matrices. Algorithms for finding the QRF quickly by exploiting sparcity patterns in matrices are covered in [26], [27]. Algorithmic improvements are easily realized once the structure of the gradient matrices in equation 25 are made clear.

The gradient of Equation 17 with respect to the regressors $\Theta = [a^T, x^T]^T$ has the structure,

$$J = \left[\begin{array}{cc} \frac{\partial f(a,x)}{\partial a} & \frac{\partial f(a,x)}{\partial x} \\ \frac{\partial (a - \hat{a})}{\partial a} & \frac{\partial (a - \hat{a})}{\partial x} \end{array} \right] \tag{27}$$

$$= \left[\begin{array}{cc} B_{n \times n} & D_{n \times 2} \\ I_{n \times n} & 0_{n \times 2} \end{array} \right] \tag{28}$$

where n is the number of data points and $B_{n \times n}$ represents a banded $n \times n$ matrix and $D_{n \times 2}$ is a dense $n \times 2$ matrix. For the energy formulation, equation 16, the matrix has three bands and for the force formulation, equation 15, the matrix has 5 bands. Techniques outlined in [26] for solving Tikhonov regularized problems, via Givens rotations for example, are easily adapted to find the least squares solution for matrices with this structure.

C. Simulation Proof of Concept

The above algorithms, run on the same truth simulation as in the linear case in figure 6, yield estimates for C_x and R_d in figure 9. The nonlinear energy and force form parameter estimates consistently estimate the longitudinal stiffness to within about 2% or 3% for data sets on the order of 600 points long. As such, there is no clear advantage in terms of estimation accuracy for one form or another. Future applications, such as direct use of the GPS velocity measurement, or parameter identification with road grade may show a stronger preference for one form over the other.

A force slip curve using linear least squares and the new method appears in figure 10. The solid line represents the true

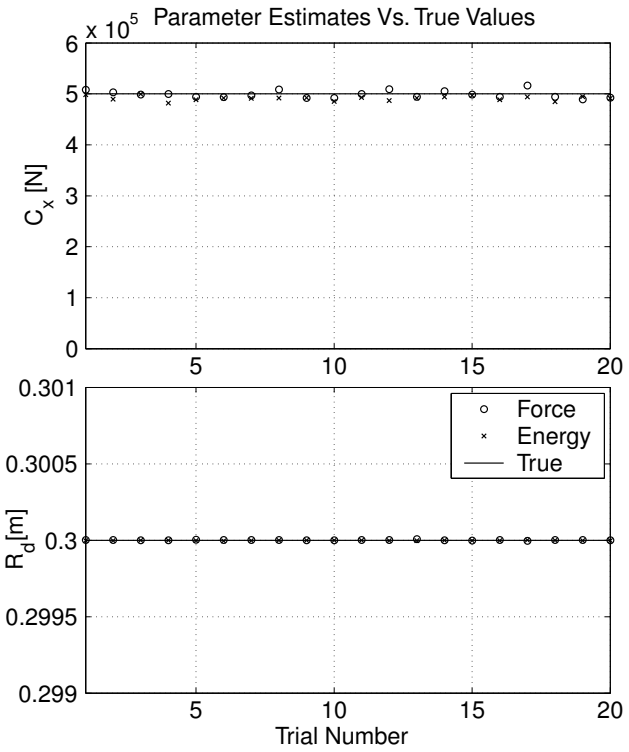

Fig. 9. Truth simulation for nonlinear parameter estimation schemes

longitudinal stiffness, the raw data are scattered about the line and normal least squares returns a biased longitudinal stiffness estimate. The dots along the true longitudinal stiffness line represent the line fit of the raw data which have been corrected by the nonlinear algorithm of Section IV. The corrected data

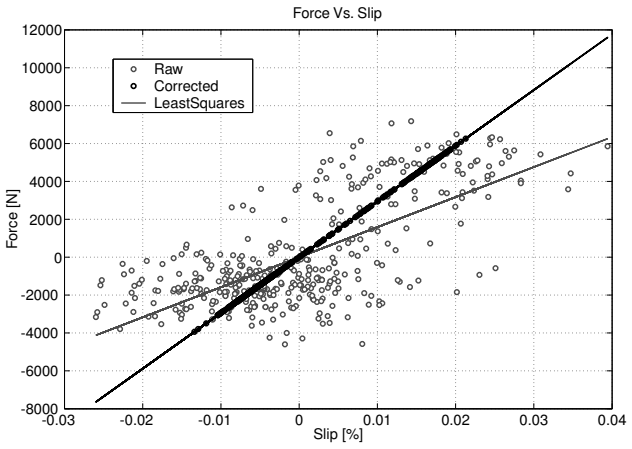

Fig. 10. Raw and corrected force-slip curves from wheelspeed sensors

are generated by subtracting the errors $\Delta\theta_u$ and $\Delta\theta_d$ from the measurements and then solving for the force and slip as in equation 2 with the approximated time derivatives from equation 13 and equation 14.

A time domain plot of the measured slip and the slip corrected with the nonlinear total least squares estimator appears in figure 11

These simulation results show that a nonlinear estimation strategy which incorporates detailed attention to the way the

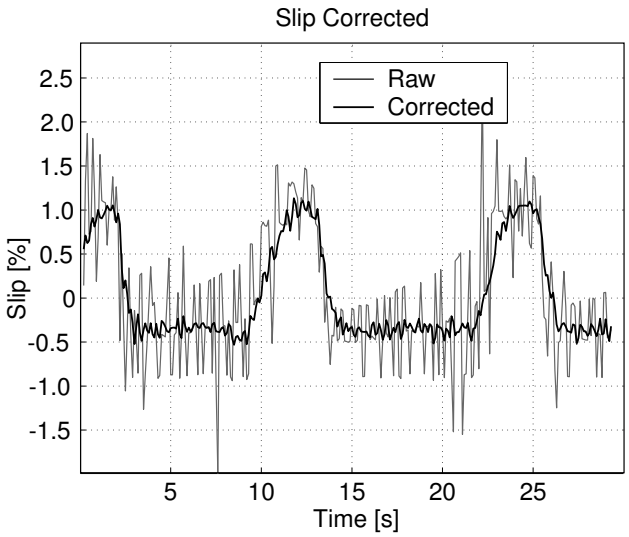

Fig. 11. Raw and corrected wheel slip for test data

noise enters the force-slip model solves many of the problems encountered with the linear formulations.

VI. Test Setup and Results

This section applies the nonlinear estimation schemes defined above to vehicle data recorded under several driving conditions.

A. Test Apparatus

For our experimental testing we are using a rear wheel drive 1999 Mercedes E320 with stock installed variable reluctance Antilock Braking System (ABS) sensors. Additional equipment includes a Novatel GPS receiver and a Versalogic single board computer running the MATLAB XPC embedded realtime operating system. This system records and processes 20 data streams comfortably at sample rates up to 1000[Hz].

Figure 12 shows a schematic of how the ABS sensors function and the signal processing used to measure wheel angular positions. As the toothed ABS gear rotates, it changes the permeability of the space near the sensor. This permeability change induces a sinusoidal current in the sensor which is then measured by the signal conditioning circuitry which is sampling at 200[kHz]. This signal conditioning then counts the number of zero-crossings of the sinusoid and transmits this number over a digital bus to the single board computer at 200[Hz].

In an effort to hold as many tire variables constant as possible, the data collected for these results were collected on the same section of asphalt on a flat, straight, dry runway parallel to eliminate the effects of turning and road grade from the measurements. Force was applied to the tires by accelerating with throttle and decelerating with engine braking only. Thus the undriven wheels were free to roll at all times. The test road has no overhanging trees or tall buildings nearby so the GPS antenna had an unobstructed view of sky and was unlikely to experience multipath errors. Wheel angular displacements were recorded at 200Hz, summed over the

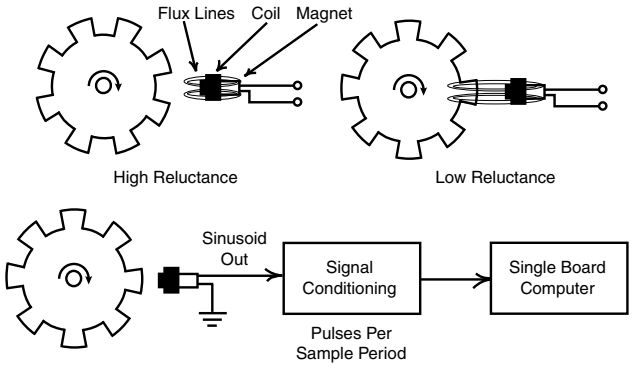

Fig. 12. Schematic of ABS sensor functionality and signal processing

length of the data set and then sub-sampled at 10Hz to reduce the auto correlation of high frequency wheel modes and reduce the computational cost of the nonlinear solution. Data sets are on the order of 600-900 points long. Figure 13 shows a typical data set for the estimation scheme. This test data compares well to the simulation data used for verification in Figure 5

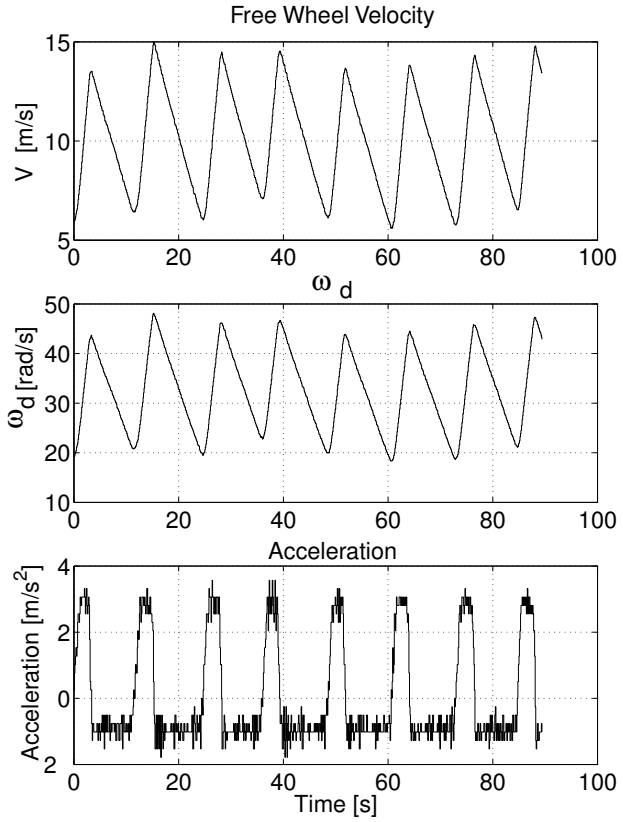

Fig. 13. Schematic of ABS sensor functionality and signal processing

To lend further support to the simulation study, Figure 14 shows typical measurement residuals returned from the estimation scheme. Although they are clearly correlated, they are also below the minimum sensor quantization resolution. This suggests that the estimation scheme is probably near the limits of sensor performance.

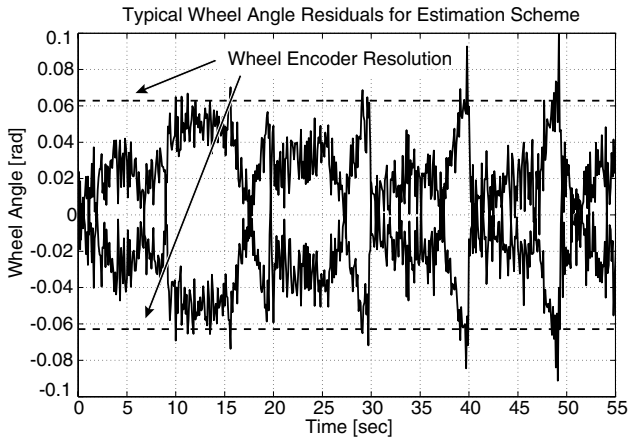

Fig. 14. Schematic of ABS sensor functionality and signal processing

Tire Test Matrix			
#	Pressure	Tread	Weight
1	nominal	full	driver only
2	-10%	full	driver only
3	-20%	full	driver only
4	nominal	2.5[mm]	driver only
5	nominal	full	driver +200[kg]
6	nominal	full	driver +400[kg]
7	nominal	full, wet	driver only

TABLE I

TEST MATRIX FOR PERFORMANCE AND WINTER TIRES

B. Test Matrix

In an effort to identify the relative importance of inflation pressure, tread depth, vehicle loading and surface lubrication for longitudinal slip estimation, the following tires:

1. ContiWinterContact TS790, 215/55 R16
2. Goodyear Eagle F1 GS-D2, 235/45 ZR17

were tested under the conditions outlined in table I. Testing a tread depth of $2.5[mm]$ shows the performance of a tire toward the end of its operational life.

C. Data Discussion

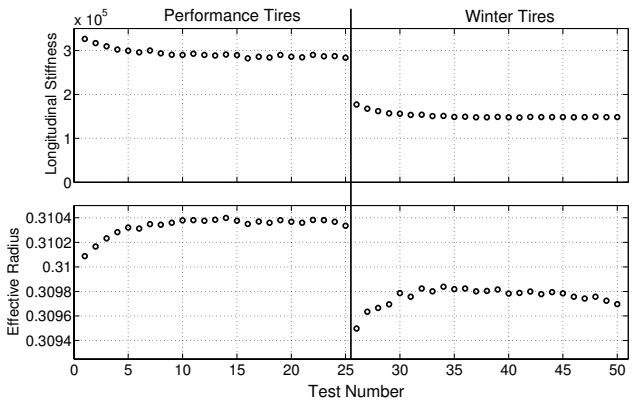

Fig. 15. Convergence of tire parameters over several identical tests

Figure 15 shows two series of 25 sets of data, with each point representing an approximately 60 [s] test run. The first

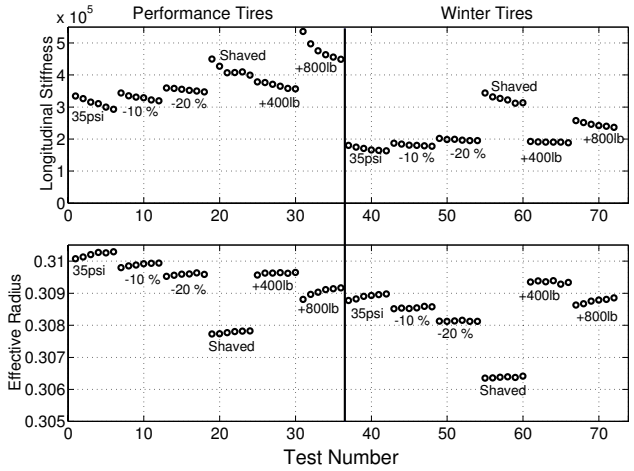

Fig. 16. Tire parameters for various testing conditions

Longitudinal Stiffness Change		
Test	Performance	Winter
Cold-hot temp	-17 %	-21 %
-10% pressure	17 %	15 %
-20% pressure	29 %	28 %
Reduced Tread	34 %	91 %
+200 [kg]	13 %	7 %
+400 [kg]	60 %	42 %
Wet Road	4 %	-2 %

TABLE II

LONGITUDINAL STIFFNESS CHANGE FROM NOMINAL

series were performed with the performance tires and the second with winter tires. The estimator is strongly consistent for consecutive data runs as the longitudinal stiffness estimates converge to steady state. The first order exponential response of the estimates is likely due to the frictional heating of the tires. This affects the tire properties in two ways. First it increases the internal pressure of the tire which tends to decrease the size of the contact patch and thus decrease the longitudinal stiffness. The second is that the rubber of the tires softens at higher temperature. This causes more deflection for the same force and therefore also lowers the longitudinal stiffness of the tire. The estimates converge when the heating due to testing is equal to the cooling while prepping for the next test run, about 6 tests.

Figure 16 shows the dependance of longitudinal stiffness upon the conditions outlined in the test matrix.

Table II shows the relative longitudinal stiffness change from nominal for each entry of the test matrix. For the case of cold-hot, the effect is adjusted to account for the $1-2$ [psi] change of the internal tire pressure due to heating. The second set of clusters in Figure 17 show 8 data sets taken after a day of rain while the road is still wet and actively sprayed with fresh water. Unfortunately, the tests had to be stopped for a few minutes to refresh the water supply on every forth run, the tire cooling during the water change explains the rise in stiffness between tests 4 and 5 during the wet tests. The influence of road lubrication is clearly smaller than that of any other influence. *It is highly unlikely that an estimator could identify this surface as particularly wet during normal driving, even if all other parameters were given.*

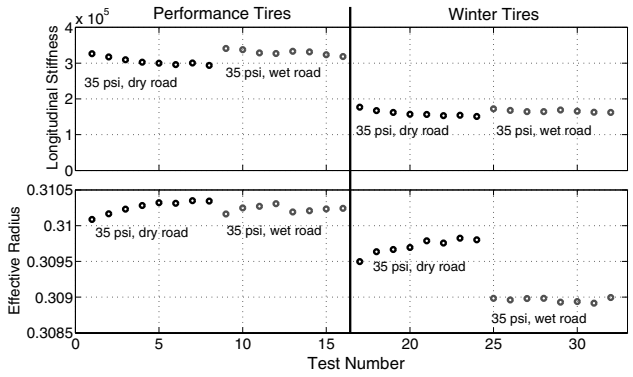

Fig. 17. Comparison of tire parameters for dry versus wet asphalt

The wheel effective radius estimates are remarkably consistent, regularly returning values with submillimeter accuracy. It is interesting to note that the wheel effective radii vary by less than one millimeter for tire pressure changes of 20%.

The snow tires exhibit the most surprising wheel radius behavior, a $\frac{1}{2}$ millimeter reduction of effective radius for the snow tires on a lubricated road surface and the increase of effective radius for higher normal loading. This and the rest of the data presented in this section suggests that tires are extremely complex and detailed care should be taken whenever inferring information solely from the lumped parameters, longitudinal stiffness and effective radius.

VII. CONCLUSIONS

Although it is common practice to place measurements in the estimation matrix for linear least squares, for this application it returns significantly biased parameter estimates. This motivates the introduction of two new nonlinear estimation schemes which appear to be unbiased when the modeling assumptions hold. Using this improved estimation strategy longitudinal stiffness and effective radius of two different kinds of tires were carefully tested under several different test conditions. The data clearly shows that there are several important parameters which govern tire longitudinal stiffness behavior. At a minimum, inflation pressure, tread depth, normal loading and temperature have a strong influence on linear longitudinal stiffness estimates for low values of slip. Interestingly, road lubrication by water had the smallest influence on longitudinal stiffness estimates of all test conditions

VIII. FUTURE WORK

Tire cornering stiffness exhibits different sensitivities to inflation pressure, tread depth and normal load than longitudinal stiffnesses [15]. It may be possible to combine sideslip [28], [16] and longitudinal slip estimators, possibly with a Bayesian network [29], such that inflation pressure and tread wear may be reliably inferred. Additionally with the recent advances toward in-tire temperature and pressure sensors, it may be possible to further isolate tread temperature and inflation pressure effects from other operating conditions.

This isolation could then enable indirect tire temperature and pressure sensing. Furthermore, if this technique shows a strong correlation between peak road friction coefficient and longitudinal stiffness estimates, then it may be applicable for road condition identification.

There are several details remaining for a practical real time implementation of a longitudinal stiffness estimator of this form. Recent work in [20] demonstrates real time mass, road grade, rolling resistance and aerodynamic drag estimation. These proposed schemes would allow slip estimation under more realistic driving conditions. Furthermore brake force modeling, pitch dynamics and incorporation of the GPS sensor into the estimation scheme will allow for slip testing under braking and on 4 wheel drive vehicles.

There appears to be little information about about wet verses dry roads embedded in tire behavior for low values of slip, however, these tests were far from exhaustive. Future work will experiment with lower peak friction surfaces and levels of slip outside the linear region.

REFERENCES

[1] T. Dieckmann, *Der Reifenschlupf als Indikator fur das Kraftschlusspotential*. TU Hannover: Dissertation, 1992.

[2] ——, "Assessment of Road Grip by Way of Measured Wheel Variables," in *Proceedings of FISITA, London*, June 1992.

[3] F. Gustafsson, "Slip-Based Estimation of Tire - Road Friction," *Automatica*, vol. 33(6), pp. 1087–1099, 1997.

[4] F. Gustafsson, M. Drevo, U. Forssel, M. Lofgren, N. Persson, and H. Quicklund, "Virtual Sensors of Tire Pressure and Road Friction," in *SAE Paper number 2001-01-0796*.

[5] W. Hwang and B.-S. Song, "Road Condition Monitoring System Using Tire-Road Friction Estimation," in *Proceedings of AVEC 2000* 5^{th} *International Symposium of Advanced Vehicle Control*, 2000, pp. 84–89.

[6] M. Ito, K. Yoshioka, and T. Saji, "Estimation of Road Surface Conditions Using Wheel Speed Behavior," in *SAE Paper Number 9438826*.

[7] Y. Nakao, H. Kawasaki, and D. Major, "Estimaton of Friction Levels Between Tire and Road," in *SAE Paper No. 2002-01-2298*.

[8] M. Uchanski, "Road Friction Estimation for Automobiles Using Digital Signal Processing Methods," Ph.D. dissertation, University of California, Berkeley, Fall 2001.

[9] K. Yi, K. Hedrick, and S.-C. Lee, "Estimation of Tire-Road Friction Using Observer Based Identifiers," *Vehicle System Dynamics*, vol. 31, pp. 233–261, 1999.

[10] C. Canudas-De-Wit and R. Horowitz, "Observers for Tire/Road Contact Friction Using Only Wheel Angular Velocity Information," in *Proceedings of the* 38^{th} *Conference on Decision and Control*, 1999, pp. 3932–3937.

[11] L. Ray, "Nonlinear Tire Force Estimation and Road Friction Identification, Simulation and Experiments," *Automatica*, vol. 33, no. 10, pp. 1819–1833, 1997.

[12] E. Rossetter and J. Gerdes, "The Role of Handling Characteristics in Driver Assistance Systems with Environmental Interaction," in *Proceedings of the 2000 ACC, Chicago, IL*, 2000.

[13] A. T. van Zanten, "Evolution of Electronic Control Systems for Improving the Vehicle Dynamic Behavior," in *Proceedings of the* 6^{th} *International Symposium on Advanced Vehicle Control*, 2002.

[14] L. Ljung, *System Identification: Theory for the User*. Upper Saddle River, New Jersey: Prentice-Hall, Inc., 1999.

[15] H. Sakai, "Theoretical and Experimental Studies on the Dynamic Properties of Tyres, part 4," *International Journal of Vehicle Design*, vol. 3, pp. 333–375, 1982.

[16] J.-O. Hahn and R. Rajamani, "GPS-Based Real-Time Identification of TireRoad Friction Coefficient," *IEEE Transactions on Control System Technology*, vol. 10, NO.3, pp. 331–343, MAY 2002.

[17] E. Bakker, L. Nyborg, and H. Pacejka, "Tyre Modelling for Use in Vehicle Dynamics Studies," in *SAE Paper 870421*, 1987.

[18] H. Dugoff, P. Francher, and L. Segel, "An Analysis of Tire Traction Properties and Their Influence on Vehicle Dynamic Performance," *SAE Document Number Document 700377*, 1970.

[19] A. van Zanten *et al.*, "Control aspects of the Bosch-VDC," in *Proceedings of AVEC 96, Aachen University of Technology, June, 1996*, 1996, pp. 573–607.

[20] H. S. Bae, J. Ryu, and J. C. Gerdes, "Road Grade and Vehicle Parameter Estimation for Longitudinal Control Using GPS," in *IEEE Conference on Intelligent Transportation Systems, Proceedings, ITSC*, 2001, pp. 166–171.

[21] D. M. Bevly, R. Sheridan, and J. C. Gerdes, "The Use of GPS Based Velocity Measurements for Improved Vehicle State Estimation," in *Proceedings of the American Control Conference, Chicago IL*, 2000, pp. 2538–2542.

[22] S. L. Miller, B. Youngberg, A. Millie, P. Schweizer, and J. C. Gerdes, "Calculating Longitudinal Wheel Slip and Tire Parameters Using GPS Velocity," in *Proceedings of the American Control Conference*, 2001.

[23] S. V. Huffel and J. Vandewalle, *The Total Least Squares Problem:Compulational Aspects and Analysis*. Philadelphia: Society for Industrial and Applied Mathematics, 1991.

[24] C. R. Carlson and J. C. Gerdes, "Identifying Tire Pressure Variation by Nonlinear Estimation of Longitudinal Stiffness and Effective Radius," in *Proceedings of AVEC 2002* 6^{th} *International Symposium of Advanced Vehicle Control*, 2002.

[25] H. Schwetlick and C. Tiller, "Numerical Methods for Estimating Parameters in Nonlinear Models With Errors in the Variables," *Technometrics*, vol. 27(1), pp. 17–24, 1985.

[26] A. Bjorck, *Matrix Computations*, 3^{rd} *edition*. Philadelphia: Society for Industrial and Applied Mathematics, 1996.

[27] G. H. Golub and C. F. V. Loan, *Matrix Computatons*, 3^{rd} *edition*. Baltimore and London: The Johns Hopkins University Press, 1996.

[28] J. Ryu, E. J. Rossetter, and J. C. Gerdes, "Vehicle Sideslip and Roll Parameter Estimation Using GPS," in *Proceedings of AVEC 2002* 6^{th} *International Symposium of Advanced Vehicle Control*, 2002.

[29] M. L. Schwall and J. C. Gerdes, "Multi-Modal Diagnostics for Vehicle Fault Detection: DSC-24600," in *Proceedings of IMECE 2001*, 2001.

PLACE PHOTO HERE

Christopher R. Carlson Biography text here.

PLACE PHOTO HERE

J. Christian Gerdes Biography text here.